

HIGH PURITY RADIOACTIVE BEAMS AT THE BEVALAC\*

J.R. Alonso, A. Chatterjee, C.A. Tobias  
Lawrence Berkeley Laboratory

ABSTRACT

Peripheral nuclear fragmentation reactions of primary Bevalac heavy ion beams are used to produce secondary beams of radioactive nuclei. The large cross section and small deflection of the projectile fragments lead to high production and delivery efficiency for these beams. Dispersive beam transport allows good separation and purification of the desired secondary beams.  $^{11}\text{C}$  and  $^{19}\text{Ne}$  beams of high purity and good intensity (almost 0.2% of the primary beam current) are presently being used for biomedical experiments.

INTRODUCTION

It is well known<sup>1,2</sup> that one of the primary interactions experienced by relativistic heavy ions is the peripheral nuclear collision. The main characteristic of this type of reaction is that only a small amount of excitation energy is imparted to the projectile--enough to cause a breakup of the nucleus, but insufficient to produce significant changes in the projectile's velocity or trajectory (see Fig. 1). These properties of peripheral reactions can be used to produce high purity beams of specific radioactive projectile fragments with intensities adequate for many experiments.

RADIOISOTOPE PRODUCTION

The secondary beam intensity and quality are dependent in large measure on the choice of target material and thickness, as well as on the specific properties of the production reaction. Figures 2-4 examine  $^{11}\text{C}$  production efficiency, and primary beam survival and multiple scattering for a primary 400 MeV/amu  $^{12}\text{C}$  beam passing through beryllium, copper and lead targets. The horizontal axis in these figures is the remaining primary beam energy. Since  $dE/dx$  values are lower for light targets, a given beam energy loss can result from passage through a much thicker low Z target. Production efficiencies are based on cross section measurements of Lindstrom et al.<sup>1</sup> The falloff in the beryllium target below 300 MeV/amu arises from the loss of  $^{11}\text{C}$  due to nuclear reactions, and the lower production rates because of the dwindling supply of primary atoms (Figure 3).

From these three figures one sees that low Z materials make the best targets for secondary beam production. Production is higher, primary beams attenuate more

\*Work supported by the Division of Biological and Environmental Research of the Department of Energy.



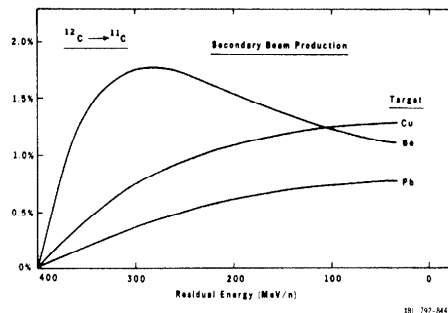
XBB 728-4219

Fig. 1. Example of a peripheral nuclear collision in emulsion (from the LBL Heckman-Greiner group). Projectile fragments all continue forward in a small opening cone, while target breakup is more closely centered about the rest frame.

rapidly and less multiple scattering (hence less beam emittance growth) occurs.

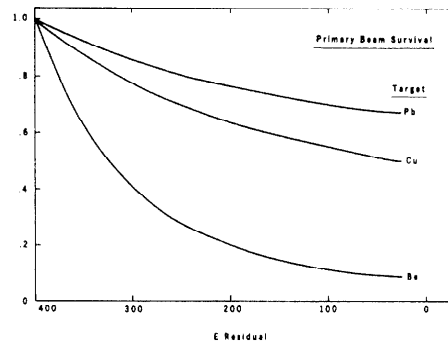
For the first runs producing  $^{11}\text{C}$  beams it was decided to use a 7.8 cm thick beryllium target. From the above calculations, expected yield of  $^{11}\text{C}$  is 1.7%, energy loss is 100 MeV/amu, primary beam survival is 40% and multiple scattering is 6 mrad.

The overall characteristics of the  $^{11}\text{C}$  beam can be predicted by combining these numbers with factors derived from the dynamics of the nuclear production



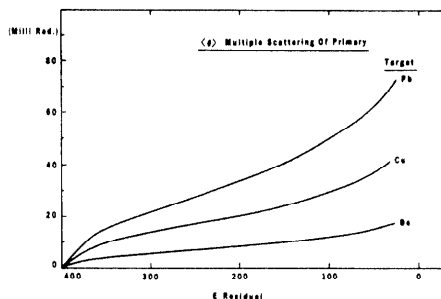
LBL 792-8440

Fig. 2. Production efficiency (as percent of total primary beam) for the single-neutron-loss projectile fragment  $^{11}\text{C}$  for different target materials, plotted against primary beam residual energy.



LBL 792-8439

Fig. 3. Survival of the primary  $^{12}\text{C}$  beam versus energy lost in different targets. Attenuation is calculated from total nuclear reaction cross sections measured by Lindstrom et al.<sup>1</sup>



LBL 792-8438

Fig. 4. Multiple Coulomb scattering of primary  $^{12}\text{C}$  beam versus energy lost for different targets. This angle must be counted along with the spreading due to the nuclear reaction to calculate emittance value of secondary  $^{11}\text{C}$  beam.

reaction. Measurements by Greiner et al<sup>2</sup> indicate that the <sup>11</sup>C is produced roughly isotropically in the projectile rest frame, and has a mean momentum value around 100 MeV/c in this rest frame. These properties were observed to be independent of beam energy and target material.

For <sup>11</sup>C production at an average energy of 350 MeV/amu, the nuclear reaction thus contributes an angular spread of about ±10 mrad, and a momentum spread of ±1%. When multiple scattering in the target is added, the net opening half-angle is 12 mrad. The target contribution to the momentum spread is about 2% (the momentum difference between a <sup>11</sup>C produced at the front of the target and degraded by the full target, and one produced at the target back by a degraded <sup>12</sup>C).

#### BEAM SEPARATION AND TRANSPORT

Figure 5 shows the beam line used for these studies. The production target is placed at F1, the first focus of the Bevatron extracted beam. The beam is brought through two bending magnets and a quad doublet to a focus at F2. The resolving power of the transport system is about 1/500, the dispersion is 14 mm per percent. Since rigidities of the <sup>12</sup>C and <sup>11</sup>C beams differ by over 10% and the primary beam spot at F2 is only a few mm across, excellent separation of the two beams is achieved. Collimators at F2 block out all but the desired <sup>11</sup>C component.

The beam line cannot transmit the full spread of the <sup>11</sup>C beam calculated above; magnet apertures restrict transmission to about 10%.

In summary, the beam delivered to the experimenter should be quite pure, with a predicted intensity ratio of about one <sup>11</sup>C atom for every 650 <sup>12</sup>C atoms striking the production target.

#### EXPERIMENTS A) <sup>11</sup>C

Figure 6 shows a Bragg ionization curve for the <sup>11</sup>C beam delivered to the Biomedical area. In this type of measurement, made with a variable thickness water absorber, each ion species exhibits a unique signature, namely a sharp peak at the end of its range. The measured range of the <sup>11</sup>C beam was 9.8 cm of water, whereas the <sup>12</sup>C beam emerging from the target had been measured earlier to have a range of 12.6 cm. The total absence of a peak at this water depth, coupled with the increased sensitivity due to considerably reduced secondary beam intensities allows us to place an estimate of suppression of the primary beam of better than 1 part in 10<sup>3</sup>.

In a parallel experiment, the beam was stopped in a block of beryllium surrounded by a sophisticated positron camera called PEBA.<sup>3</sup> This instrument recorded the radioactive decay of the stopped beam; the position of

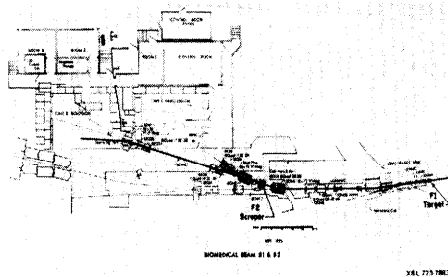


Fig. 5. Bevalac beam line to Biomedical areas. Production target is placed at F1, beam is bent and focused to F2 where scrapers isolate the secondary beam component. Further elements transport beam to experimenter in Cave II.

the stopped beam corresponded to the same range as the peak in Figure 6, the measured half-life agreed well with the 20 minute <sup>11</sup>C value, and furthermore, the specific activity measured was in agreement with the total number of recorded particles traversing the beam monitoring ionization chambers directly upstream of the beryllium block. The beam was unmistakably a very pure <sup>11</sup>C beam. The beam flux monitored in the experimental area was typically 2 x 10<sup>7</sup> ions per pulse, for a flux at F1 of 1.5 x 10<sup>10</sup> <sup>12</sup>C ions per pulse, or about 1 part in 750, close to the calculated predictions.

#### B) <sup>19</sup>Ne

In another experiment, a beam of <sup>19</sup>Ne was produced from an incident <sup>20</sup>Ne beam, the measured Bragg curve is shown in Figure 7. The characteristics of the (<sup>20</sup>Ne, <sup>19</sup>Ne) reaction are sufficiently similar to those for carbon that calculated transmission factors are essentially identical. Slightly lower cross sections are compensated for by slightly less divergence owing to higher initial projectile momenta. In actual fact, the observed intensity ratio was very close to that seen for <sup>11</sup>C.

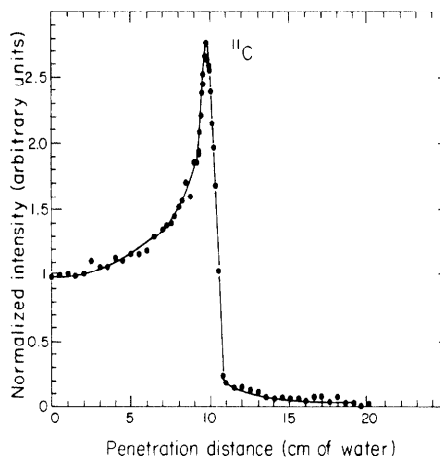


Fig. 6. Bragg ionization curve of <sup>11</sup>C beam showing that beam stopped after passing through 9.8 cm of water. No evidence is visible of primary <sup>12</sup>C beam (range measured at 12.6 cm), indicating excellent separation at F2.

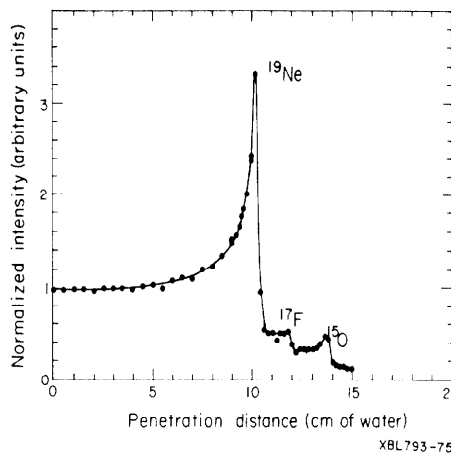


Fig. 7. Bragg curve for <sup>19</sup>Ne produced from <sup>20</sup>Ne. Contaminants are <sup>17</sup>F and <sup>15</sup>O which, because of similar Z/A values and overlapping momentum distributions could not be separated from <sup>19</sup>Ne.

Note that although a peak at the  $^{20}\text{Ne}$  range (11.0 cm) is totally absent, two well-defined satellite peaks are seen. These ranges correspond to  $^{17}\text{F}$  and  $^{15}\text{O}$ , which have similar charge-to-mass ratios as  $^{19}\text{Ne}$ , and because of overlapping momentum distributions cannot be separated from the  $^{19}\text{Ne}$  with the present beam line. Separation of these contaminants could be achieved by using a degrader at F2 (producing different energy losses for the three different ion species), and then using the bending element B2M1 to spatially separate the three components.

#### BEAM AVAILABILITY

These radioactive beams are now a part of the regular Bevalac beam inventory. Parameters and tuning conditions have been established, so that once the primary beam is extracted to F1 it is only a matter of a few minutes to insert the target, scale transport magnets and set collimators before the beam is ready for experimental use.

#### USES OF RADIOACTIVE BEAMS

Positron emission, the decay mode of  $^{11}\text{C}$  and  $^{19}\text{Ne}$ , allows one to easily pinpoint the location of the nuclear disintegration, i.e., the point where the beam particle stopped. The positron stops within a short distance of its parent (typically less than 1 mm), and annihilates, producing two 511 keV photons given off in opposite directions. A matrix of detectors placed around the beam stopping point observes both photons and so places the decay point along the line of these photons. The observation of many such lines allows one to calculate their intersection point, and hence the location of the actual source of the activity. The PEBA detector,<sup>3</sup> with 72 NaI crystals, has been used for all the studies to date, and is capable of measuring beam stopping points with an accuracy of  $\pm 1$  mm.

The uses of these beams of positron emitters fall into two broad areas, nuclear medicine and radiotherapy treatment planning verification. Present and envisioned applications of radioactive beams in nuclear medicine diagnostic procedures are numerous. For example, implantation of radioactive atoms at any specified location of the body with a bolus-determined pattern with subsequent measurement of the level of activity at the same site will provide a technique for

the determination of the micro-circulation in vital organs. This could yield useful information on the physiological condition in such areas as heart-valve actions, the nervous system, etc. Implantation experiments with  $^{11}\text{C}$  beams have already been done using dogs. In one example, the radioactivity was deposited in the carotid artery and blood-flow mapping was done in the brain.

The greatest potential value of these beams, however, will be in the localization of the Bragg peak in relation to the tumor volume to be treated. This verification is of utmost importance for effective heavy particle cancer radiotherapy. It is difficult to calculate the density of tissue through which the beam must pass before stopping because variations in the amount of bone, blood, fat, air, tissue, etc. to be penetrated. CT scans dramatically improve treatment planning, although the treatment verification precision will still be inadequate in a number of cases.

Using the available radioactive beams and the PEBA detector, experiments are now underway to detect stopping point variations in phantoms of different shapes and inhomogeneities. Preliminary data with the  $^{11}\text{C}$  and  $^{19}\text{Ne}$  beams indicate that positioning verification of the Bragg peaks of the primary  $^{12}\text{C}$  and  $^{20}\text{Ne}$  beams can be done with an accuracy of  $\pm 1$  mm. This technique will soon be tested with animals and will be evaluated and developed for use in human cancer therapy.

#### ACKNOWLEDGMENTS

We wish to acknowledge the assistance of Jorge Llacer for performing beam measurements with PEBA, Dr. E. Alpen for continuing support of our work and interest in developing uses for the beams, and Marsh Tekawa and the Bevalac operations staff for assistance in beam delivery and tuning.

#### REFERENCES

1. P.J. Lindstrom, D.E. Greiner, H.H. Heckman, B. Cork, F.S. Bieser, LBL-3650, Feb. 1975.
2. D.E. Greiner, P.J. Lindstrom, H.H. Heckman, B. Cork, F.S. Bieser, Phys. Rev. Letters 35 (1975) p. 152.
3. J. Llacer, A. Chatterjee, H.C. Jackson, J.C. Lin, M.V. Zunzunegui, LBL-8138 (1978).